

Geo-atmospheric processing of airborne imaging spectrometry data

Part 1: parametric orthorectification

Daniel Schläpfer

1) Remote Sensing Laboratories (RSL), Department of Geography,
University of Zurich, CH - 8057 Zurich / Switzerland,
Phone: +41 1 635 52 50, Fax: +41 1 635 68 46,
E-mail: dschlapf@geo.unizh.ch, <http://www.geo.unizh.ch/~dschlapf>,

2) ReSe Applications Schläpfer, Langeggweg 3, CH - 9500 Wil / Switzerland
<http://www.rese.ch>

Rudolf Richter

DLR - German Aerospace Center, Remote Sensing Data Center
D - 82234 Wessling / Germany

ABSTRACT

An operational orthorectification solution in support of the combined geometric and radiometric processing of currently available imaging spectrometry data is presented. The described parametric geocoding procedure (PARGE) strictly considers the aircraft and terrain geometry parameters and uses a forward transformation algorithm to create orthorectified imaging spectrometry cubes. The implementation principles, the auxiliary data calibration strategies, and the workflow of the currently applied processor are discussed. The major error sources of the approach are identified, and possibilities are shown how to make the most out of the available auxiliary data (INS/GPS) parameters. Results on HyMap and AVIRIS imaging spectrometry data show an absolute accuracy in the range of 1-3 pixels for this kind of imagery. The combination of PARGE with an atmospheric correction procedure is shown in part 2 to this paper. The depicted geo-atmospheric workflow is proposed as standard processing approach for available and future imaging spectrometry data.

1. Introduction

Geometrical and radiometrical effects account for the main distortions present in imaging spectrometry data and need to be corrected for a physics-based validation of the imagery. The prerequisite for the correction of most radiometrical and atmospheric effects is an accurate description of the scanning geometry for every pixel of the raw image.

This situation led to a joint effort of the Remote Sensing Laboratories (RSL), University of Zurich, and the German Aerospace Establishment (DLR) Wessling in synchronizing two independent procedures for geometric and atmospheric processing and their optimization with regard to the specific characteristics of airborne imaging spectrometry data. Such a smooth 'geo-atmospheric' processing chain is also a powerful tool for radiometric processing of other, well-calibrated optical remote sensing data. The relevant orthorectification procedure is described in this paper whereas the atmospheric correction part is explained in a second paper in this issue (Richter and Schläpfer 2001).

Airborne optical scanner images suffer from distortions due to the sensor movement during data acquisition. Even mechanically stabilizing platforms built into the carrier can not remove these effects completely as residual movements of the stabilizing systems remain. These distortions become relevant if pixel- or even sub-pixel accuracy is required. For non-stereographic imagery (as acquired by most of the current imaging spectrometers), a physically exact representation of the scan geometry can be obtained by the parametric geocoding approach as presented here.

State of the art

Orthorectification of airborne electro-optical scanner data can be solved using various approaches. Traditional polynomial 'rubber sheet' approaches (e.g., Bähr 1976, Goshtasby 1988) require a large number of tie-points to account for sensor movements and often do not achieve satisfying accuracies for airborne data (McGwire 1996). Although piece wise polynomial models offer a promising potential even for airborne data, they can not solve for all high frequency distortions in the image (except if linear features of the image are employed (Lee et al., 2000)). On the other hand, correlation matching algorithms (Devereux et al. 1990, Börner 1999, Reulke et al. 1997, Sörgel and Thönnessen 1999) can deliver adequate results if the image is structured. The raw image is automatically fit to orthophoto imagery. Only little human interaction is required for correction of mis-matching points. However, the latter approach only leads to satisfying results if an orthophotos or another equivalent database is available (Gregory et al. 1999).

The parametric approach is a favourable solution for imaging spectrometry data since it does not require any referenced image data sources. Parametric solutions have been implemented for satellite

imagery taking into account the respective sensor models and orbit parameters initially for Landsat MSS by Bähr (Bähr 1976) and later by Sawada (Sawada et al. 1981), then for SPOT HRV (Konecny et al. 1987), and generic orbits (Salamonowicz 1986). With all these approaches, the number of Ground Control Points (GCPs) could be significantly reduced in comparison to the pure ‘rubber-sheet’ approaches while increasing accuracy. The achieved accuracies for the satellite data as described in the above papers was between 0.5 and 1.5 pixels. The envisaged geometrical accuracy for airborne imaging spectrometry is pixel-accuracy after geocoding. This requirement is defined as an absolute pixel position accuracy being better than 50% of the actual pixel size. At a nominal spatial resolution of actual instruments between 4 and 20 meters, the generic accuracy requirement is in the range of 2 to 10 meters.

Parametric models have already been implemented for various airborne scanners: e.g., AISA (Bärs et al. 1999); AVIRIS (Boardman 1999); CASI (Wilson et al. 1997, Staenz et al. 1998), and Daedalus ATM AADS-1268 (Brewster 1999, Mockridge and Leach 1997). An in-depth evaluation of these methods is beyond the scope of this paper. The current status and detailed methodology used in the mentioned methods may be obtained directly from the respective authors.

The motivation of the herewith presented work was to implement a flexible generic methodology for parametric orthorectification with special emphasis on the requirements of currently used airborne imaging spectrometry data (such as AVIRIS and HyMap). Hence, it has to deal with the intrinsic data quality of these sensor systems and its associated auxiliary data. The created “Parametric Geocoding” procedure (PARGE) reconstructs the scanning geometry for each image pixel using position, attitude, and terrain elevation data. A first version of the model has been created at RSL starting in 1992 (Meyer 1994) as an AVIRIS specific tool. It then evolved to a generic application including extensive GCP based calibration procedures (Schläpfer et al. 1998a/b). However, it bears the potential of complete automation if the auxiliary data are provided absolutely calibrated in space.

2. Methodology

The first fundamental equations describing the airborne scanning geometry have been derived by Derenyi and Konecny (1966) and further refined by Konecny (Konecny 1976a, 1976b). For this paper, a calculation approach has been chosen which does not make use of the collinearity equations directly (Konecny 1972) but is capable to use the collinearity condition on each parameter individually to increase the accuracy of the results.

Geometric model

The scan process can be geometrically described by a linewise data acquisition with one auxiliary parameter set per image line for position ($x / y / z$) and attitude (roll ω / pitch φ / heading κ). This description includes two approximations: First, the orientation of the camera to the aircraft can be neglected if the attitude angles are measured directly on the sensor head, and the DGPS information has been corrected for the distance between GPS antenna and sensor head. Secondly, the scan period for whiskbroom scanners between the first and the last pixel in an image line is neglected if only one auxiliary data set per image line is available. Furthermore, it is assumed that the sensor model is aligned to the IMU system within 2 degrees (compare accuracy considerations on page 13). Such pragmatic approximations are allowed in order to stay within the required accuracy for airborne imaging spectrometry data as given above (± 2 -10 meters).

The geometric model applied in this paper starts with the scan vector \vec{L}_0' as seen in the sensor intrinsic coordinate system. The corresponding initial coordinate system is taken such that it corresponds directly to image coordinates, having the x' ('pixel') direction across track and the y' ('line') direction along track (see figure 1). Note that this coordinate system is not in line with the common definitions used in classic photogrammetry. It rather has been chosen specifically for the line scanner situation such that the x -coordinate corresponds to the scan movements.

[put figure 1 here]

The geometric sensor model for the scanning system assumes that all across track scan vectors lie in a co-planar system. The initial scan vector per pixel can then be derived directly from the pixel scan angle as:

$$L_{0,x}' = s \tan(\theta), L_{0,y}' = 0, \text{ and } L_{0,z}' = -1, \quad (1)$$

where θ is the relative scan angle between pixel scan vector and nadir, and s is the sign being negative for left hand side (in flight direction) pixels. The parameter $L_{0,y}'$ is zero for this starting situation (compare remarks on the geometric sensor model on page 13). The sensor coordinate system is now rotated by the attitude angles according to the measurement order of the three angles. This rotation leads to new coordinates of the scan vector \vec{L}_0 in the digital elevation model (DEM) coordinate system:

$$\vec{L}_0 = \mathbf{R} \cdot \mathbf{P} \cdot \mathbf{H} \cdot \vec{L}_0', \quad (2)$$

what is written explicitly as:

$$\begin{bmatrix} L_{0,x} \\ L_{0,y} \\ L_{0,z} \end{bmatrix} = \begin{bmatrix} \cos\omega & 0 & -\sin\omega \\ 0 & 1 & 0 \\ \sin\omega & 0 & \cos\omega \end{bmatrix} \begin{bmatrix} 1 & 0 & 0 \\ 0 & \cos\varphi & \sin\varphi \\ 0 & -\sin\varphi & \cos\varphi \end{bmatrix} \begin{bmatrix} \cos\kappa & \sin\kappa & 0 \\ -\sin\kappa & \cos\kappa & 0 \\ 0 & 0 & 1 \end{bmatrix} \cdot \begin{bmatrix} L_{0,x}' \\ L_{0,y}' \\ L_{0,z}' \end{bmatrix} \quad (3)$$

$$= \begin{bmatrix} \cos\omega\cos\kappa - \sin\omega\sin\varphi\sin\kappa & \cos\omega\sin\kappa + \sin\omega\sin\varphi\cos\kappa & -\sin\omega\cos\varphi \\ -\cos\varphi\sin\kappa & \cos\varphi\cos\kappa & \sin\varphi \\ \sin\omega\cos\kappa + \cos\omega\sin\varphi\sin\kappa & \sin\omega\sin\kappa - \cos\omega\sin\varphi\cos\kappa & \cos\omega\cos\varphi \end{bmatrix} \cdot \begin{bmatrix} s \tan(\theta) \\ 0 \\ -1 \end{bmatrix} \quad (4)$$

where \mathbf{R} , \mathbf{P} and \mathbf{H} are the coordinate transformation matrices for the attitude angles roll (ω), pitch (φ), and true heading (κ), respectively. The parameters ω and φ are interchanged in the above equations in comparison to standard definitions (Konecny and Lehmann 1984) due to the scanner-compatible coordinate system. Note that the true heading κ is defined to direction north in counter clock-wise sense which is opposite to the geographic direction standard.

The scan vector length has finally to be constrained to the aircraft altitude in order to obtain the real-length scan vector \vec{L}_t :

$$\vec{L}_t = \frac{-h}{L_{0,z}} \vec{L}_0 \quad (5)$$

The above equations describe, how the coordinate system is virtually turned from the aircraft system to the actual position (Konecny and Lehmann 1984, Denker 1996). This kind of transformation is contrary to the rotation methods as usually applied in digital photogrammetry (e.g., Zhang et al. 1994).

Ray tracing

An orthorectification process has to consider the terrain elevation in a precise manner using a ray tracing algorithm and a DEM, starting at the aircraft position $\vec{P}_{air}(t)$. The ray tracing intersects the effective view line with the DEM (see figure 2). First the view line within the altitude range of the DEM (minimal height h_{min} , maximal height h_{max}) is created. Its starting point \vec{P}_S and ending point \vec{P}_G are defined as

$$\vec{P}_S = \vec{P}_{air} + \frac{h - h_{max}}{h} \vec{L}_t, \text{ and } \vec{P}_G = \vec{P}_{air} + \frac{h - h_{min}}{h} \vec{L}_t, \quad (6)$$

where h is the aircraft altitude above ground (compare figure 2). The new intersection line \overline{SG} is defined between these two points. Its vertical projection on the DEM surface is now calculated by creating a profile

along the trace of the vector. The highest intersection point $\overrightarrow{P_{pix}}$ between \overline{SG} and the profile is now found by comparing the altitudes of both lines on an equally spaced basis. The horizontal coordinates of $\overrightarrow{P_{pix}}$ can then be stored as final result of the geocoding process (while its altitude is now available directly from the DEM).

This forward ray tracing procedure provides a pixel-accurate intersection point position. It is specifically suited for airborne scanning situations where backward intersection (propagation from the DEM) is less efficient due to the linewise changing geometry. Moreover, the procedure is able to solve for the problem with multiple intersections of the view line with the DEM since the highest intersection point is taken first.

[put figure 2 here]

Parameter offset determination

Theoretically, all sensor-parameters used for the presented calculation may be systematically offset by a certain amount due to misalignment of the sensor to the attitude measurement system or due to systematic inaccuracies of the aircraft position measurement system (usually a GPS). PARGE uses a statistical approach based on a number of GCPs to calculate individual offsets for roll, pitch, heading, or the aircraft position. While currently available GPS systems provide accurate positions, the attitude measurements and the altitude are the ones which most likely are affected by certain offsets.

For every GCP, the difference between real and estimated GCP position is calculated using the collinearity condition. After rotating the coordinate system back to the heading direction, the offsets for roll angle (across track direction) and pitch angle (along track direction) can be calculated for every GCP. The generic roll and pitch offsets are now calculated as average of all angular offsets at the GCPs. A few iterations are required to minimize these offsets since roll and pitch are not independent parameters in the rotation matrix. Offset on roll and pitch in the range of $\pm 3^\circ$ can be corrected using this approach without being in error more than 0.1 mrad (i.e. at small angles, offsets to the coordinate rotation can replace a change to the sensor model within this accuracy, compare figure 3). If higher offsets are observed, the sensor model needs to be changed to account for the misalignment between attitude gyros and sensor optical axis.

[put figure 3 here]

For the heading and the altitude offsets, the statistical relation between angular offset at all GCPs to the distance from the nadir pixel is evaluated. The roll offset per GCP correlates to the distance from nadir,

if the altitude is in mistake. Such an offset may be realistic for certain GPS receivers, since the altitude measurement is the least accurate of all three parameters. The correlation between nadir distance and roll offset is thus minimized iteratively with the altitude offset, converging to a stable solution. The analogous technique is used to retrieve heading offsets, where the correlation between nadir distance and pitch offset is minimized. In order to converge to an optimal solution, roll and pitch offsets always need to be reiterated after a correction for altitude or heading has been applied.

The approach described for roll and pitch could also be applied to the x/y offsets where no iterations are required between the two parameters. The potential correction of such shifts in position would lead to various solutions of the same problem and is therefore avoided – the position should be accurate enough given the currently available GPS systems. More details on the above described procedure can be found in Schläpfer et al. (1998b).

Resampling

The orthorectification procedure retrieves the centre pixel positions for each imaged pixel. This output has to be resampled to achieve a regular grid. For the imaging spectrometry data, nearest neighbour approaches are preferred in order to avoid spatial interpolation (this would lead to not-measured, ‘unphysical’ spectra, compare also part 2 to this paper). Spectral integrity is thus preserved and is given higher priority than spatial quality and smoothness. However, new investigations by the authors* have shown that spatial interpolation should be preferred for the resampling of direct neighbour pixels, if more priority is put on geometric accuracy and not on spectral integrity. The nearest neighbours are derived by Delaunay triangulation (IDL 1999) or by optional fast buffering algorithms based on the output centre pixels. The advantage of the triangulation is a higher accuracy if more than 1 final resolution pixels need to be filled.

The geometric panorama effects (larger pixel footprints at off-nadir positions) are corrected satisfactorily by the nearest neighbour resampling techniques. Radiometric panorama effects do not need to be considered because the sensor characteristics are constant for every pixel if an electro-mechanical ‘whisk-broom’ scanner is employed for data acquisition. For future hyperspectral pushbroom instruments such as APEX (Itten et al. 1997), the IFOV (Instantaneous Field of View) may slightly vary across track and can therefore cause radiometric panorama effects. Such influences will have to be measured by the laboratory calibration procedure and be corrected in the data calibration process (Schläpfer et al. 1999).

* paper to be presented at VERIDIAN airborne remote sensing conference 2001, San Francisco.

3. Implementation

The implementation of a parametric geocoding procedure has to take into account a number of specialities with respect to imaging spectrometry data. First, a common architecture for the geocoding process and the data entities has to be defined for the broad variety of sensors and scan scenarios. Secondly, tools have to be provided which allow importing, quality analyses, filtering, synchronizing, and recalibration of the auxiliary data. Ground control points are used to determine the absolute calibration of the airplane attitude angles, average height and position. Finally, special side outputs are defined for efficient further processing of the data and for a smooth link to the radiometric processing environment.

The whole implementation of PARGE has been designed using IDL® (IDL 1999) and is based on ENVI™ (ENVI 1999) data formats. Thus, the application is platform-independent and can easily be integrated in a standard imaging spectrometry data processing environment. A widget-based graphical user interface for the whole functionality and a contextual on-line help system further support the end user. The program's internal data format contains image, sensor, and DEM attributes, as well as all sets of auxiliary data. The format helps to reconstruct the processing steps and to store intermediate status reports. It is designed in a generic way such that it is easily adaptable to any airborne scanner.

Input data

By definition, any parametric approach relies on physically measured auxiliary data. The requirements for the indispensable input data are summarized in table 1. The critical parameters for the procedure include the geometric sensor model and the synchronization uncertainty in addition to the six classical orientation parameters. The minimal accuracy requirement for each parameter is derived equivalent to a pixel accuracy of one fifth of the pixelsize under standard geometric conditions. Furthermore, the estimated technically feasible accuracy for most parameters is listed (ESA, 2000). The goal of this limit is to obtain pixel accuracy of the final results.

[put table 1 here]

The most critical parameters (as seen in table 1) are sensor model, synchronization, and the three attitude angles. Since these parameters are physically approximately independent, the overall practically achievable accuracy ΔP for a 0.5 mrad IFOV instrument is

$$\Delta P = \sqrt{\sum(\Delta p_i^2)} \approx 0.38 \text{ pixels} \quad , \quad (7)$$

which is well below the theoretically required ± 0.5 pixels as required for ‘pixel-accuracy’. The individual deviations Δp_i are the horizontal pixel position errors as given in Table 1.

All coordinates of the DEM and the airplane position have to be transformed consistently to a metric rectangular geodetic coordinate system in order to make use of the above formulation of the geometric model. The spatial resolution of the DEM is chosen based on the nominal pixel size of the image since the DEM definition initiates the final resolution and extent of the geocoded image.

Process workflow structure

The process workflow of the PARGE procedure has been implemented based on the requirements of well-known hyperspectral sensors such as DAIS 7915 (Chang et al. 1993), AVIRIS (Vane and Goetz 1988), or HyMap (Cocks et al. 1998). A major goal was to create an interactively usable application with a full set of flexible features between raw input data and orthorectified image output. The interactive elements are required due to the experimental character of some distributed data formats and the mediocre quality of some currently available imaging spectrometry auxiliary data. Nevertheless, all computing steps are available in a scripting environment for integration in fully operational processing chains.

[put figure 4 here]

The workflow structure is depicted in figure 4. The first steps of the workflow are concerned with the data preparation of image, auxiliary, and DEM data. Interactive viewing and filtering capabilities support this section of the process. The raw imagery is preferably transformed to a band sequential (BSQ) data format in the beginning to ease further geometric processing. The information loss in the geocoding process is minimized by resampling the DEM (defining the final image) to a slightly higher spatial resolution than the nominal resolution of the original image data.

A number of GCPs is required for validation and recalibration of the auxiliary parameters. Even in generally well documented test sites that are overflown with high performance sensors, the alignment of the IMU system to the sensor may be slightly offset. The parameter offset determination as described in section 2 of this paper is necessary for all three above-mentioned airborne imaging spectrometry systems and is therefore part of the ‘standard’ processing flow.

In practice, parts of the auxiliary data may be corrupted to some extent. The flightpath (x/y) or roll/pitch may then be interpolated based on GCP-based algorithms (Schläpfer et al. 1998a), as long as a good measurement of the remaining parameters exists. The interpolations need an increased number of GCPs in the range of 1 GCP per 100-200 scan lines for a geometric quality at about 3-5 pixels. Image areas with

less GCPs will suffer from low geometric quality. A number of iterations between parameter interpolation and the offset algorithms (up to 5) are required to converge to a satisfying solution. Cubic spline interpolation is applied for the flightpath reconstruction process due to the continuous characteristics of the flight trajectory. On the other hand, the highly variable angular roll and pitch movements of the aircraft can only be roughly approximated by linear interpolation. Of course, the finally achieved geometric accuracy after such interpolations is mediocre compared to the exact solution but the method helps to make the most out of the available data. Heading and altitude variation can not be easily interpolated using such algorithms. Their respective offsets could only be approximated if two or more GCPs are available within the same scan line or within a number of 'stable' scan lines (group of lines where the respective parameter is approximately constant). Thus, only offsets are derived for these two parameters.

A consistency check concludes the data preparation, giving clues to missing or non-compatible parameters and data. The whole auxiliary data status can now be saved for documentation and later re-iteration of the auxiliary parameters preparation. The main processing algorithm as described in the methodology section of this paper is the next step. First, the image pixel coordinates (original pixel and line number) are written to an array in DEM geometry at their geocoded position. This results in a 'mapping array' which is stored as main output of the processing. In parallel, the viewing geometry per image pixel is saved to a separate file which is described in detail below. The effective production of geocoded images is the last step to be performed. The mapping array is applied directly to the original image data, to perform the final geocoding. This process is used to create RGB images for visualization and accuracy assessment as well as for full orthorectified image cubes. The mapping array may also be applied to processed thematic results in order to avoid the large storage capacity overhead of geocoded imaging spectrometry data.

Processing timeframe

The whole processing (work and computing) can take between less than an hour for seamless standard approaches up to days per scene. A typical image of 512 x 2000 pixels needs 10-20 minutes processing time of on a Macintosh G3 or a Sun workstation for the geometric part, and another 5-15 minutes for the production of a geocoded cube consisting of 200 bands (cube size: input 0.5 GB, output approx. 1 GB). The total required processing time increases proportionally with the number of lines to be processed.

The effort for the data preparation highly depends on the quality of the auxiliary data and the accuracy requirements of the data end user. Correct auxiliary data synchronization and the correct conversion of the DGPS data to the DEM geometry may require sophisticated (external) tools and specific cartographic knowledge and programs. The introduction of the GCPs is the part of the workflow which introduces a considerable amount of uncertainty and which is time critical if highest possible accuracies are

required. A careful GCP validation and selection has to be done as in all GCP-based geocoding procedures. Conversely, the fully scriptable environment of PARGE allows the definition of a standard processing workflow which theoretically does not need any human interaction. This fastest approach requires as little as half an hour of CPU time per image run plus the time for the data handling.

Link to radiometric processing

The scan angles output provides all the linking layers for later radiometric processing of the geocoded image (cf. Schläpfer et al. 1998c). It includes three data layers in DEM resolution describing the relative geometry between airplane and observed pixel: the scan zenith (being negative for pixels on the right hand side of the nadir), the absolute scan azimuth to direction north, and the height of the aircraft (see figure 5). The scan azimuth is required for the correction of BRDF effects and the aircraft altitude is provided for completeness of the geometric description. Further radiometrically relevant geometric parameters which only depend on the DEM such as slope, aspect, and elevation are calculated separately prior to the radiometric correction. The scan angle output can be directly fed into ATCOR4 which is the airborne version of the atmospheric correction approach ATCOR (Richter 1998). The description of this method used for terrain dependent radiometric processing of imaging spectrometry data is given in part 2 of this paper (Richter and Schläpfer, this issue).

[put figure 5 here]

4. Accuracy evaluation

An increasing number of remote sensing applications such as GIS based modelling require pixel accuracy for imported information layers. High spatial accuracy is also required if in-flight calibration experiments have to be performed (Schaepman et al. 1997). The approach presented here bears the potential to achieve this goal or high resolution airborne imaging spectrometry data. However, a number of errors given below have to be minimized.

DEM related errors

DEM resolution and georeferencing accuracy are major error sources in the orthorectification process. Taking into account the residual height of vegetation and buildings, the inaccuracies increase since standard DEMs seldomly represent the observed surface. The vertical accuracy of a DEM can be easily related to the resulting horizontal orthorectification accuracy depending on the scan zenith angle. A short analysis of the DEM-related horizontal error is shown in table 2.

[put table 2 here]

Airborne imaging spectrometers typically have a FOV (Field of View) between ± 15 degrees and ± 30 degrees and spatial resolutions between 4 and 20 meters. Thus, the critical vertical DEM accuracies to achieve pixel accuracy as given in table 2 are between 5 meters (e.g. HyMap case) and 50 meters (e.g. AVIRIS high altitude case). These errors are equivalent to the typical height of buildings or trees. For high quality results in standard European landscapes it is therefore advantageous to use high accuracy digital surface models for orthorectification instead of ground elevation based DEMs.

Auxiliary data error sources

The requirements to the auxiliary data have already been given in table 1. Some critical details to the individual parameters are given below because each of these parameters can lead to corrupt results if it is affected by errors.

- *GPS/DGPS*

The flightpath of the aircraft as well as ground control points are usually measured with GPS/DGPS systems. The required accuracies as given in table 1 can be easily achieved with current DGPS systems. Special care has to be taken in the cartographic transformation of the GPS coordinates to the geodetic coordinate system of the DEM, where systematic errors up to hundreds of meters may occur. Such transformation errors may arise if e.g. an user uses an inappropriate datum for his coordinate system or if inaccurate software is used for that purpose. If non-differential GPS is used for data acquisition, the altitude becomes inaccurate to 10 to 50 meters and potential offsets or drifts in horizontal position have to be taken into account.

- *Roll and Pitch*

The attitude can be measured to sub-pixel accuracy down to 0.09 mrad using high end IMU systems (e.g. with the Applanix System, Hutton et al. 1997). However for low to medium cost systems (such as the C-MIGITS, Skaloud et al. 1997), the alignment offset between sensor and IMU is often not accurately adjustable and thus needs to be reconstructed using GCPs (compare section below on sensor description). The accuracy of low cost systems is in the range of 1 mrad for short term data acquisitions. For long image runs (i.e. longer than 1 min.), the attitude parameters may also be affected by drifts. A GCP-based drift correction for roll or pitch can therefore lead to an improvement of results within long line data acquisitions. As

the GPS system have become very accurate, the absolute and relative accuracy of the attitude measurement system still is a major problem for the herein investigated imaging spectrometry systems.

- *Heading*

The absolute true heading (i.e. the angle between sensor orientation and DEM direction north) may suffer from the absolute accuracy of the IMU systems, since in currently available systems its accuracy is lower by a factor 2-4 in comparison to roll and pitch. Also, the heading is often not transposed during the coordinate conversion step what may lead to errors if there is a cartographic declination between 'true' direction north and the north direction at local coordinates.

The approximation of one parameter set per scan line for whiskbroom scanners introduces another small systematic error to the heading in the range of 0.1° (compare 'geometric model' section on page 4). This error can be reduced by adjusting the geometric sensor model. If this is not done, the effects can be partially removed by correcting the heading offset from a number of GCPs.

- *Synchronization*

The perfect synchronization of the auxiliary data to the image lines is a difficult task in sensor construction. The instrument master clock needs to be exactly registered for each image line during data acquisition for that purpose. A variety of synchronization errors may occur: apparent drifts in the auxiliary data appear if the synchronization is done based on the data acquisition frequency instead of explicit time tags per image line. Offsets between the auxiliary data stream and the image data are likely if two separate clocks are used during data acquisition or if the read-out of the master clock is delayed against the data acquisition. Exact knowledge of the mechanism for the instrument master clock registration is required to solve this problem.

For whiskbroom scanners, one can argue that the measurement of all parameters per image pixel (rather than per line) is desirable to further increase accuracy. As the current scanners scan between 12 and 25 Hz, such an approach only is valuable if highest quality and high frequency (200 Hz and more) attitude measurement units are available and if the synchronization is perfect to the millisecond. This approach has not been further followed by the authors so far, but may be included in future systems.

- *Geometric sensor model*

A final error source is the description of the sensor itself, the so-called 'sensor model'. The exact knowledge of the lines of sight to every across-track pixels is crucial for an exact solution of the problem. An equally spaced distribution of the pixels across track is given for regular whiskbroom scanners as described in this paper. The geometric sensor model for a non-moving whiskbroom instrument can thus be described

as given in equation (1). This model may be changed to account for the movement of the sensor during the scan process of one line. The related effect is similar to a heading offset and can also be corrected by applying a correction to the heading angle as described above. Thus the sensor model does not depend on the flight speed. On the other hand, the pixels are not necessarily equally spaced across track and the lines of sight may form a non-planar system. The inclusion of such instrument characteristics in the parametric geocoding process therefore requires a high quality geometric laboratory calibration to assess the lines of sight to every spatial element.

Earlier in this paper (section 2) the potential misalignment between sensor and IMU has been described. This misalignment can be corrected in PARGE by adding offsets to the measured attitude angles. In reality, such a misalignment could also be treated as part of the sensor model, where the respective lines of sight are adjusted by the offset angles independently. This leads to a comprehensive solution since the rotational transformation as given in Equation (3) can afterwards be applied absolutely in parallel to the IMU measurements. An example of the difference of the introduction of offsets in the sensor model instead of applying them to the rotation angles is given in figure 3. Misalignment below 3° can be adjusted to a very high accuracy by applying them to the rotation angles. Higher misalignments (e.g. modelling a physically tilted sensors) on the other hand need to be taken into account by adjusting the sensor model.

Accuracy assessment

The accuracy of the orthorectified results can be assessed using various approaches. The most common method is the consideration of residuals from independent GCPs (McGwire 1996) while correlation analysis of the results to reference images is a more robust approach (Congalton 1988).

The accuracy of the parametrically geocoded imagery is assessed using four approaches:

- calculate the location residuals of ground control points which were not used for the prior calculation,
- correlation analysis of the results to the DEM based illumination map (as required for atmospheric correction),
- correlation analysis of digital maps to the geocoded results,
- correlation analysis of co-registered imagery taken at different days.

The spatial correlation analyses are made based on a regular sampling grid between the result image and a reference image of exactly the same resolution and extent. The herewith retrieved accuracies can be attributed directly to the accuracy of the engaged input data due to the parametric approach.

5. Results for AVIRIS and HyMap imagery

The PARGE procedure has been applied to a broad variety of airborne imaging spectrometry data such as DAIS 7915, HyMap, AVIRIS, and others. Each sensor has its own problematic specialities what has lead to the high degree of flexibility in the current application.

The DAIS 7915 imaging spectrometer has been operated by DLR Oberpfaffenhofen on a regular basis (Müller and Oertel 1997). It is originally equipped with some built-in gyros of relatively low absolute accuracy. A high accuracy IGI IMU (IGI Ltd., Hilchenbach, Germany) and a DGPS unit have therefore been mounted for most data acquisition runs. A misalignment between IMU and optical axis of the sensor remained which could be detected and removed using the offset technique given on page 6. Geocoding accuracies within ± 2 pixels accuracy can be achieved based on standard DEMs. These results of the processing for DAIS data have already been given in Schläpfer (1998b) and are not explained in more detail in this paper.

The achieved results for example AVIRIS and HyMap scenes are given in the next sections. The two examples are representatives for two kind of data: The AVIRIS data of 1998 are of experimental character with respect to their geometric quality. This data set is mainly used to test the flexibility and limitations of the PARGE software for critical imaging spectrometry data. The HyMap data on the other side are processed on a regular basis using the PARGE application. The respective results correspond to the real-world accuracies which can be achieved on a truly operational basis.

AVIRIS

Already the initial development of the PARGE application had been based on AVIRIS data. Recently, it has been the new low altitude option flying AVIRIS on a Twin Otter aircraft (Green et al. 1999) which pushed the demand for parametric georectification again. AVIRIS registers the earth surface at a FOV of 31.2° and 1mrad IFOV from altitudes between 3 and 21 km. A full-parametric standard rectification procedure has been introduced for AVIRIS by Boardman (Boardman 1999) which however does not include orthorectification capabilities. Additional geometric processing is required to retrieve orthorectified images from these standard products. Hence, the methodology described in this work has been adapted and tested on standard raw AVIRIS data products in order to provide a ‘one-step’ orthorectification procedure for this instrument. The workflow differs between high altitude data and low altitude data due to the distinct GPS/INS configurations and the difference in aircraft characteristics.

For high altitude data, only the ER-2 aircraft information for position and attitude is available, synchronized to the AVIRIS data stream. The heading is taken as derivative of the (non-differential) GPS-

flightpath. The low frequency pitch variations are interpolated over best-known GCPs (since pitch is not measured so far for the sensor head) and overlaid to the high frequency pitch measurements. Both parameters require some smoothing filtering to remove measurement artefacts. Another problem is the software roll compensation which has been applied to the standard AVIRIS high altitude data: the provided aircraft roll parameters are no longer relevant for processing. Analysis using a number of GCPs however have shown, that significant residual roll variations within 0.5 degree remain in the data. The roll variations have therefore to be interpolated from GCPs. All the above assumptions are applicable since the aircraft is flying at 20 km altitude under very stable conditions and the data do not suffer from large distortions.

For low altitude data acquisition, a Boeing C-MIGITS II IMU has been mounted on the AVIRIS sensor head starting in 1998. This system is comparable in accuracy to the unit used on the HyMap sensor (see next section) and measures the position and attitude to at best 1 pixel accuracy. The use of this auxiliary data for currently available AVIRIS data sets can be very time-consuming; specifically since the synchronization offset between attitude measurements and image lines is not known exactly and since the IMU data formats are inconsistent between the years. The external GPS and attitude data have to be synchronized using (an often varying) offset to the AVIRIS master clock.

An experimental data set has been investigated with both high altitude data (flown at 21 km altitude) and low altitude data (at 3.7 km altitude) acquired over the Ray Mine site, Arizona, in summer and fall 1998 (McCubbin and Lang 1999). A standard USGS DEM with a horizontal resolution of 30 meters is used as surface reference. It is resampled to the required output resolutions for both data sets, and registered to the UTM (North American datum 1927) coordinate system. The processing has been done using the standard PARGE methods, with 28 GCPs for the high altitude data and 18 GCPs for the low altitude scene. The results of co-registration of the two AVIRIS data sets is shown in figure 6. The relative accuracy between the two images has been assessed by correlation analysis from image to image and from images to the illumination shaded DEM (as described in the section on accuracy assessment on page 14). All given accuracies are of relative character since no absolute geometric standard could be established for the test area. Overall relative accuracy turns out to be stable throughout the high altitude and low altitude flight-lines which consist of 1478 and 4487 contiguous scan lines, respectively. The observed relative shifts between the three co-registered data layers were between 15 and 40 meters. This accuracy is low when comparing to the low altitude pixel size (3.75m), but is within the estimated accuracy for the high altitude data where no accurate flight parameters were available.

The residuals of the GCPs indicate an error in the range of 10 -15 m (3-5 pixels) for the low altitude scene while the high altitude residuals are in the range of 20-30 meters. The low altitude data accuracy suffered from the incomplete system integration and synchronization, the low DEM resolution, and from

drifts on the pitch parameter which needed to be corrected. The accuracy still bears the potential for improvement if higher quality DEMs or surface models would be used. Anyhow, the results are within an acceptable margin given the fact that only a small number of GCPs had to be used. Tests of the software capabilities on more recent AVIRIS data containing completely synchronized attitude and DGPS information will be done as soon as such data are available.

[put figure 6 here]

HyMap

Orthorectification of HyMap data has only been envisaged recently as the data of this Australian sensor has become available to a broad community of users in Europe. Having a large FOV of 61.44° at an IFOV of 2 mrad, orthorectification is a must for this sensor if the radiometry shall be corrected in dependence of the geometry. An IGI Inertial Navigation System has been mounted on the HyMap sensor head for dedicated campaigns in Europe in 1998 and 1999. Although the IGI system is of high accuracy, this setup was flawed by the missing system integration and cumbersome synchronization to the HyMap imaging spectrometer. In mid 1999, a Boeing C-MIGITS system was finally integrated to the HyMap system as standard measurement unit. The accuracy of this system is in the range of 1 mrad for roll and pitch and down to 3 mrad for heading (Skaloud et al. 1997). It decreases with longer flightlines, since it may be affected by slight drifts. Hence at best it is possible to achieve pixel-accurate geocoding using this INS data.

One main goal of the campaign in Barrax 1999 (organized and funded by the European Space Agency (Berger et al. 2000)) was to measure the spectral variability of agricultural areas under varying geometric flight conditions. Six overlapping data sets has been taken over the same area. These data sets have been co-registered using the PARGE application under operational conditions and based on a flat, artificial DEM. The achieved accuracy as derived from the residuals of 15 GCPs was between 7 and 10 meters.

An example of the differences between two co-registered images is shown in figure 7. Variations of the gray level within the difference image can be attributed to the BRDF effects due to the 90 degree difference in flight heading. The strong appearance of some field borders on the other hand can be clearly attributed to the co-registration errors between the two images. The RMS co-registration errors have been assessed by cross-correlation analysis of all six images. The horizontal offsets have been searched by systematic correlation analysis on a regular raster of 100 pixel width, spread over the overlapping image size. Up to 10% of the test points have been excluded from the offset calculation if no correlation maximum could be found within 10 pixels vicinity. This has been the case if the correlation is searched within mostly

homogeneous agricultural fields (e.g.) or if the surface characteristics changed between two acquisition dates. The results are summarized in table 3 and an example is shown in figure 7. According to the table, the co-registration error for this HyMap imagery is between 1.3 and 2.2 pixels which corresponds to 6.5 to 11 meters. This result confirms the residuals as derived from the GCPs.

[put table 3 here]

The observed error can be attributed to the non-availability of a digital surface model and the moderate quality of the IGI INS system integration (alignment/synchronization) with HyMap used in 1998. Also, the number of GCPs was restricted to 15 per scene and the processing had been done using PARGE in an operational environment at the German Aerospace Centre (DLR) without much room for extensive re-iteration efforts. The results could be further optimised by adding in-field measured GCPs in relevant areas and by optimising the parameter offsets to fit the best GCPs. Results from other HyMap scenes where a number of 30 and more GCPs had been used showed GCP residuals down to 3 meters, which might be the practical accuracy limit for this sensor/INS combination.

[put figure 7 here]

6. Conclusions

A parametric geocoding methodology has been presented which currently is used for operational processing of hyperspectral data by various European Institutions. It allows for the correction of attitude and flightpath dependent distortions in airborne imagery and offers interactive GCP-based auxiliary data calibration capabilities. Current imaging spectrometers such as AVIRIS, DAIS, and HyMap are supported, while further airborne systems may be taken in the system later. The procedure proved to be flexible and operationally applicable for all these instruments, even for data sets with partially corrupted or incomplete auxiliary data.

Although the theoretical accuracy of the method is in the sub-pixel range, current real world accuracies for the three investigated imaging spectrometer systems are in the range of 3 to 20 meter (1-3 pixels). This accuracies can be improved substantially, as higher quality DEMs, DSM (surface models), GPS, and attitude data measurements become available for these instruments. The availability of high accuracy GCPs is another prerequisite for an improved calibration of auxiliary data. The experiences from these tests can help in the definition of future airborne imaging spectrometers such as APEX.

AVIRIS data geocoding leads to satisfactory results even if standard USGS DEMs are used. Digital elevation models of higher accuracy combined with a highest quality completely integrated INS/GPS unit would substantially increase the accuracy of the geocoding of low altitude data. The results are nevertheless better than those achieved with traditional georeferencing methods, specifically over rugged terrain. The results for HyMap data are substantially better because of the more accurate synchronization of the auxiliary data to the imagery and the availability of differential GPS for the flightpath determination.

The PARGE application is successfully joined with the radiometric and atmospheric correction package ATCOR4. Both software packages are currently available as commercial products*. This integration of the geometric and atmospheric correction processes is an important step towards a completely physics-based preprocessing chain for imaging spectrometry data.

* more information about the availability of PARGE and ATCOR4 can be found at <http://www.rese.ch>.

7. Acknowledgements

We acknowledge the contributions of the following persons to this work: Gabriela Strub, Stephan Bojinski, Michael Schaepman (all with the RSL), and Andrea Hausold (DLR). The European Space Agency (ESA) is acknowledged for the HyMap data and the Jet Propulsion Laboratories Pasadena and Rob Green are thanked for the AVIRIS data. The study has been supported by Prof. Klaus I. Itten from the Remote Sensing Laboratories of the University of Zurich.

8. References

- BÄHR, H.P., 1976, Geometrische Modelle für Abtasteraufzeichnungen von Erderkundungssatelliten. *Bildmessung und Luftbildwesen*, 44(5):198-204.
- BÄRS, R., WATSON, L., and WEATHERBEE, O., 1999, AISA as a tool for timely commercial remote sensing. 4th international airborne remote sensing conference and exhibition, ERIM, Ottawa, CA, Vol. I:239-246.
- BERGER, M., MORENO, J., MÜLLER, A., SCHAEPMAN, M., WURSTEISEN, P., RAST, M., and ATTEMA, E., 2000, The digital airborne imaging spectrometer experiment – DAISEX '99. IG-ARSS 2000, Hawaii, Vol. VII:3039-3041.
- BREWSTER, S.B., 1999, Geometric correction system capabilities, processing, and applications. 4th international airborne remote sensing conference and exhibition, ERIM, Ottawa, CA, Vol. I:162-169.
- BOARDMAN, J., 1999, Precision geocoding of low altitude aviris data: lessons learnt in 1998. R. Green (Ed.), 8th Annual JPL Airborne Earth Science Workshop, Pasadena, CA, JPL 99-17:63-68.
- BÖRNER, A., 1999, Entwicklung und Test von Onboard-Algorithmen für die Landfernerkundung. Inst. für Weltraumsensorik und Planetenerkundung, DLR Berlin, ISRN DLR-FB--1999-19, pp. 122.
- CHANG, S.-H. , WESTFIELD, M.J., LEHMANN, F., OERTEL, D., and RICHTER, R., 1993, 79-Channel airborne imaging spectrometer. *Imaging Spectrometry of the Terrestrial Environment*, Orlando, SPIE 1937:164-172.
- COCKS, T., JENSSEN, R., STEWART, I., WILSON, I., and SHIELDS, T., 1998, The HyMap™ airborne hyperspectral sensor: the system, calibration and performance. *Proceeding of the 1st Earsel Workshop on Imaging Spectroscopy, EARSeL/RSL, Zürich*, pp. 37-42.
- CONGALTON, R.G., 1988, A comparison of sampling schemes used in generating error matrices for assessing the accuracy of maps generated from remotely sensed data. *Photogrammetric Engineering and Remote Sensing*, 54(5):593-600.
- DENKER, J.S., 1996, See How It Flies. Book available from World Wide Web: <http://www.mouth.com/~jsd/how>, ISBN 7016405, chapter 19
- DERENYI, E.E., and KONECNY, G., 1966, Infrared scan geometry. *Photogrammetric Engineering*, 32(5):773-779.
- DEVEREUX, B.J., FULLER, R.M., CARTER, L., and PARSELL, R.J., 1990, Geometric correction of airborne scanner imagery by matching delaunay triangles. *International Journal of Remote Sensing*, 11(12):2237-2251.

- ENVI, 1999, The Environment for visualizing images, Version 3.1, Research Systems, Inc., Boulder, Colorado, USA.
- ESA, 2000, APEX phase B final reports. Remote Sensing Laboratories, Univ. of Zürich, Switzerland, CD-Rom.
- GOSHTASBY, A., 1988, Registration of images with geometric distortions. *IEEE Transactions on Geoscience and Remote Sensing*, 26(1):60-64.
- GREEN, R.O., CHRIEN, T.G., SARTURE, C., EASTWOOD, M., CHIPPENDALE, B., KURZWEIL, C., CHOVIK, C.J., and FAUST, J.A., 1999, Operation, calibration, georectification, and reflectance inversion of NASA's Airborne Visible/Infrared Imaging Spectrometer (AVIRIS) four- and two-meter data acquired from a low-altitude platform. R. Green (Ed.), 8th Annual JPL Airborne Earth Science Workshop, Pasadena, CA, JPL 99-17:177-188.
- GREGORY, S., HEDGES, P., and ELGY, J., 1999, The geometric correction of airborne line-scanner imagery. 4th International Airborne Remote Sensing Conference and Exhibition, ERIM, Ottawa, CA, Vol. I:178-185.
- HUTTON, J.J., SAVINA, T., and LITHOPOULOS, E., 1997, Photogrammetric applications of Applanix's position and orientation system (POS). presented at the 3rd International Airborne Remote Sensing Conference and Exhibition, Applanix Corp., Copenhagen (DK), pp. 11 (separatum).
- IDL, 1999, Interactive data language (IDL), Version 5.3, Research Systems, Inc., Boulder, Colorado, USA.
- ITTEN, K.I., SCHAEPMAN, M., DE VOS, L., HERMANS, L., SCHLAEPFER, H., and DROZ, F., 1997, APEX-Airborne prism experiment a new concept for an airborne imaging spectrometer. Proc. of the Third International Airborne Remote Sensing Conference and Exhibition, ERIM International Inc., Copenhagen (DK), Vol. I:181-188.
- KONECNY, G., 1972, Geometrical aspects of remote sensing. Int. Congress of Photogrammetry, Commission IV, Ottawa, Invited Paper, pp. 47.
- KONECNY, G., 1976a, Mathematical models and procedures for the geometric restitution of remote sensing imagery. XIII. Int. Congress of Photogrammetry, Commission III, Helsinki, Finland, Invited Paper, pp. 33.
- KONECNY, G., 1976b, Mathematische Modelle und Verfahren zur geometrischen Auswertung von Zeilenabtaster-Aufnahmen. *Bildmessung u. Luftbildwesen*, 44(5):188-197.
- KONECNY, G., and LEHMANN, G., 1984, Photogrammetrie. de Gruyter Lehrbuch, Walter de Gruyter, Berlin / New York, pp. 393.
- KONECNY, G., LOHMANN, P., ENGEL, H., and KRUCK, E., 1987, Evaluation of SPOT imagery on

- analytical photogrammetric instruments. *PE & RS*, 53(9):1223-1230.
- LEE, C., THEISS, H.J., BETHEL, J.S., and MIKHAIL, E.M., 2000, Rigorous mathematical modeling of airborne pushbroom imaging systems. *Photogrammetric Engineering and Remote Sensing*, 66(4):385-392.
- MCCUBBIN, I., and LANG, H., 1999, Mapping Environmental Contaminants at Ray Mine, AZ. R. Green (Ed.), 8th Annual JPL Airborne Earth Science Workshop, JPL 99-17:287-290.
- McGWIRE, K.C., 1996, Cross-validated assessment of geometric accuracy. *Photogrammetric Engineering and Remote Sensing*, 62(10):1179-1187.
- MEYER, P., 1994, A parametric approach for the Geocoding of Airborne Visible/Infrared Imaging Spectrometer (AVIRIS) Data in Rugged Terrain, *Remote Sensing of Environment*, 49:118-130.
- MOCKRIDGE, W., and LEACH, M., 1997, Integrating a Deadalus 1268 ATM, attitude GPS and AHRS to achieve scan rate geometric correction. *Proceedings of the 3rd International Airborne Remote Sensing Conference and Exhibition, ERIM International Inc., Copenhagen (DK), Vol. I:158-165.*
- MÜLLER, A., and OERTEL, D., 1997: DAIS large scale facility, the DAIS 7915 imaging spectrometer in an european frame. *Proceedings of the Third International Airborne Remote Sensing Conference and Exhibition, ERIM International Inc., Copenhagen (DK), Vol. II, pp. 684-691.*
- REULKE, N., REULKE, R., SCHAEPMAN, M., SCHLÄPFER, D., STROBL, P., and MÜLLER, A., 1997, Geometric correction of hyperspectral scanner data with simultaneously acquired stereo data. E.P. Baltsavias (Ed.), *Joint ISPRS Commission III/IV, Vol. 32, Part 3-4W2, Stuttgart (G)*, pp 9-14
- RICHTER, R., 1998, Correction of satellite imagery over mountainous terrain. *Applied Optics, Optical Society of America*, 37(18):4004-4014.
- RICHTER, R. and SCHLÄPFER, D., 2001, Geo-atmospheric correction of airborne imaging spectrometry data. Part II: Atmospheric and topographic correction. *International Journal of Remote Sensing* (this issue).
- SALAMONOWICZ, P.H., 1986, An analytic correction method for satellite MSS geometric distortions. *Photogrammetric Engineering and Remote Sensing*, 52(4):491-499.
- SAWADA, N., KIDODE, M., SHINODA, H., ASADA, H., IWANAGA, M., WATANABE, S., MORI, K.-I., and AKIYAMA, M., 1981, An analytic correction method for satellite MSS geometric distortions. *Photogrammetric Engineering and Remote Sensing*, 47(8):1195-1203.
- SCHAEPMAN, M., SCHLÄPFER, D., STROBL, P., and MUELLER, A., 1997, Ground Spectroradiometric measurements in support of the validation of the calibration of the digital airborne imaging spectrometer (DAIS 7915) Data. *3rd International Airborne Remote Sensing Conference and Ex-*

- hibition, ERIM, Copenhagen, Vol. I:217-223.
- SCHLÄPFER, D., MEYER, P., and ITTEN, K.I., 1998a, Parametric geocoding of AVIRIS data using a ground control point derived flightpath. Summaries of the Seventh JPL Airborne Earth Science Workshop, JPL, Pasadena (CA), 97-21, Vol. 1:367-372.
- SCHLÄPFER D., SCHAEPMAN M., and ITTEN K.I., 1998b, PARGE: Parametric geocoding based on GCP-calibrated auxiliary data. Descour, M.R. and Shen, S.S., Imaging Spectrometry IV, SPIE Vol. 3438:334-344.
- SCHLÄPFER, D., SCHAEPMAN, M., and ITTEN, K.I., 1998c, Level II pre-processing concept for the airborne PRISM experiment (APEX). Proceeding of the 1st Earsel Workshop on Imaging Spectroscopy, EARSeL/RSL, Zürich, pp. 89-96.
- SCHLÄPFER, D., SCHAEPMAN, M., BÖRNER, A., and ITTEN, K.I., 1999, Calibration concept for the airborne PRISM experiment (APEX). 4th International Airborne Remote Sensing Conference and Exhibition, ERIM, Ottawa, CA, Vol. II:8-15.
- SKALLOUD, J., LI, Y.C, and SCHWARZ, K.P., 1997, Airborne testing of C-MIGITS II - low cost integrated GPS/IN. International Symposium on Kinematic Systems in Geodesy, Geomatics and Navigation (KIS97), Banff, Canada, pp. 161-166.
- SÖRGEL, U., and THÖNNESEN, U., 1999, Automatic geocoding of high value targets using structural image analysis and GIS data. EUROPTO, SPIE Vol. 3871:10-18.
- STAENZ, K., SZEREDI, T., AND SCHWARZ, J., 1998, ISDAS - A system for processing/analyzing hyperspectral data. Canadian Journal of Remote Sensing., 24(2):99-113.
- VANE, G. and GOETZ, A.F.H., 1988, Terrestrial imaging spectroscopy. Remote Sensing of Environment, 24:1-29.
- WILSON, A.K., MOCKRIDGE, W., and ROBINSON, M.-C., 1997, Post-processing to achieve radiometric and geometric correction of ATM and CASI data. 3rd International Airborne Remote Sensing Conference and Exhibition, ERIM International Inc., Copenhagen (DK), Vol. I:447-454.
- ZHANG, W., ALBERTZ, J., and LI, Z., 1994, Rectification of airborne line-scanner imagery utilizing flight parameters. First International Airborne Remote Sensing Conference and Exhibition, Strasbourg (F), Vol. II:447-456.

TABLES

Table 1. Parametric geocoding data entities, accuracy requirements, and potential accuracy based on standard hyperspectral sensor characteristics and currently available technology.

Group	Parameter	Description	Accuracy Requirement ^a	Potential Real Accuracy	Position Error Δp_i
Sensor	Sensor model	Theoretic view angle θ per pixel center	0.1 mrad	≈ 0.05 mrad	0.10 pixel
	Sync	Accuracy of synchronization	8 ms	≈ 5 ms	0.14 pixel
	IMU alignment	Difference between sensor optical axis and IMU main axis	16 mrad (1°)	8 mrad (0.5°)	0.08 pixels
DGPS	x/y	Aircraft coordinates	0.8 m	0.1 m	0.03 pixel
	z	Aircraft altitude	3 m	0.3 m	0.02 pixel
	Transform	Transformation to local coordinates	0.1 m	0.01 m	see text
Attitude	combined roll/pitch	Attitude per image line	0.1 mrad	0.15 mrad	0.30 pixel
	heading	True heading to direction north	0.6 mrad	0.4 mrad	0.13 pixel
DEM / DSM	altitude	Surface accuracy	3 m	0.1 m	see Section 4
	position	in alignment to the flightpath	0.8 m	0.1 m	see Section 4

a. for IFOV=0.5 mrad / Resolution = 4m / FOV = ± 15 degree / Frequency 25 Hz / Flight altitude 5 km

Table 2. Horizontal accuracy in relation to the off-nadir scan zenith angle and the DEM vertical error Δh .

Off-Nadir Scan Angle	$\Delta h = 5m$	$\Delta h = 10m$	$\Delta h = 20m$	$\Delta h = 50m$	$\Delta h = 100m$
10°	0.9	1.8	3.6	8.8	17.6
15°	1.3	2.7	5.4	13.4	26.8
20°	1.8	3.6	7.3	18.2	36.4
30°	2.9	5.8	11.5	28.8	57.7
40°	4.2	8.4	16.8	41.9	83.9

Table 3. Cross correlation offset analysis between six co-registered HyMap Images of varying heading (west or south) and day-time. RMS values of the image-to-image offsets in pixels at a pixelsize of 5 m after geocoding.

	south, 12 UTC	south, 15 UTC	west, 9 UTC	west, 12 UTC	west, 15 UTC
south, 9 UTC	1.75	1.50	2.11	1.56	1.37
south, 12 UTC	0	2.16	1.94	1.56	1.66
south, 15 UTC		0	2.16	1.84	1.36
west, 9 UTC			0	2.29	1.44
west, 12 UTC				0	1.60

FIGURES

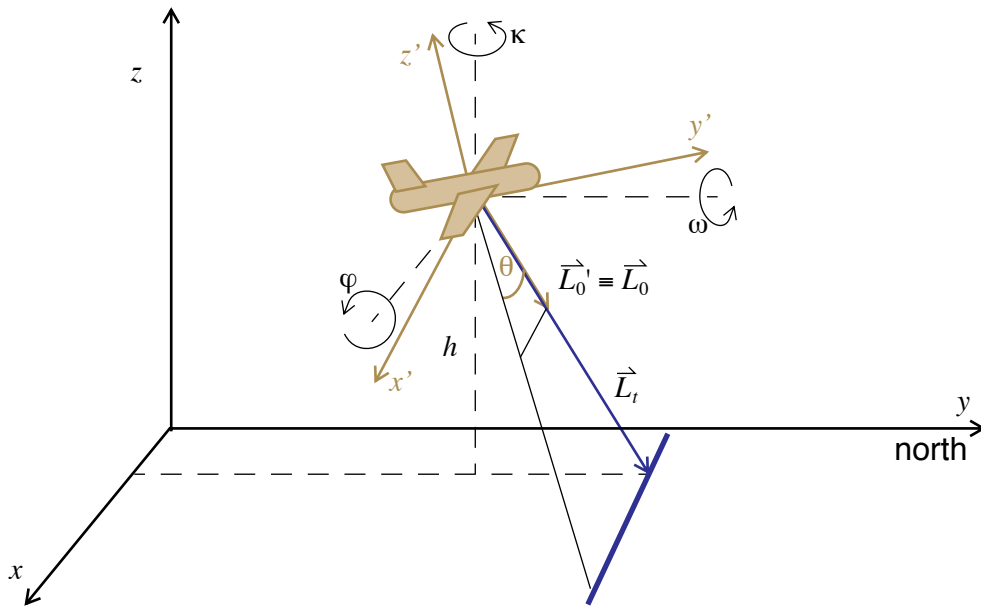


Figure 1: Rotated sensor coordinate system (x', y', z') in space and the orientation of the attitude angles $(\omega, \varphi, \kappa)$. The scan vector \vec{L}_t is derived by transformation of the coordinate system.

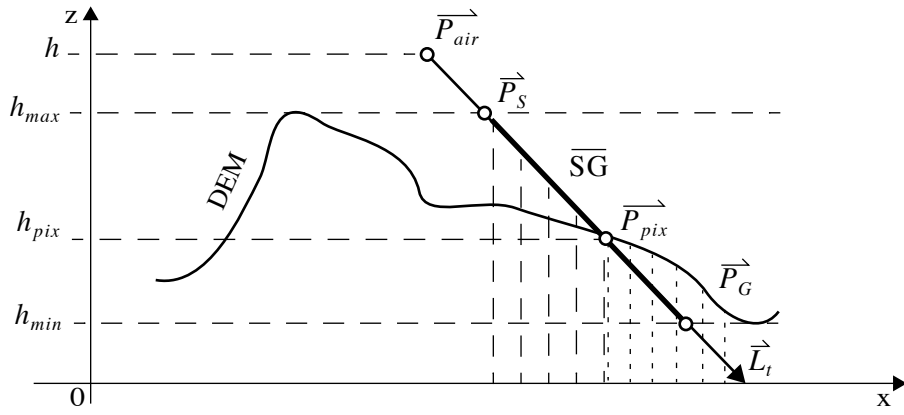


Figure 2: Intersection procedure of the real scan vector with the DEM.

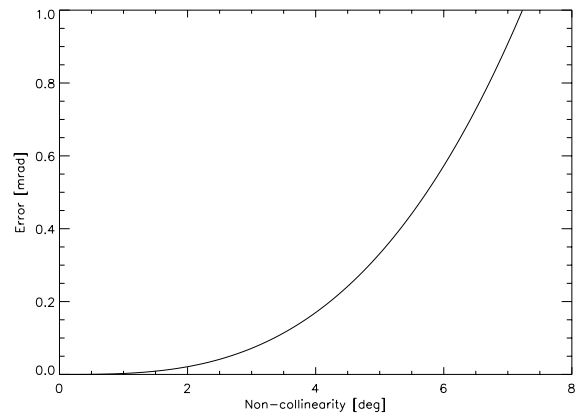


Figure 3: Error within the PARGE approach with respect to misalignment between sensor model and the attitude measurement unit. The angular difference between the exact solution (offsets directly in the sensor model) and the approximative solution with offset in the roll/pitch angles is depicted.

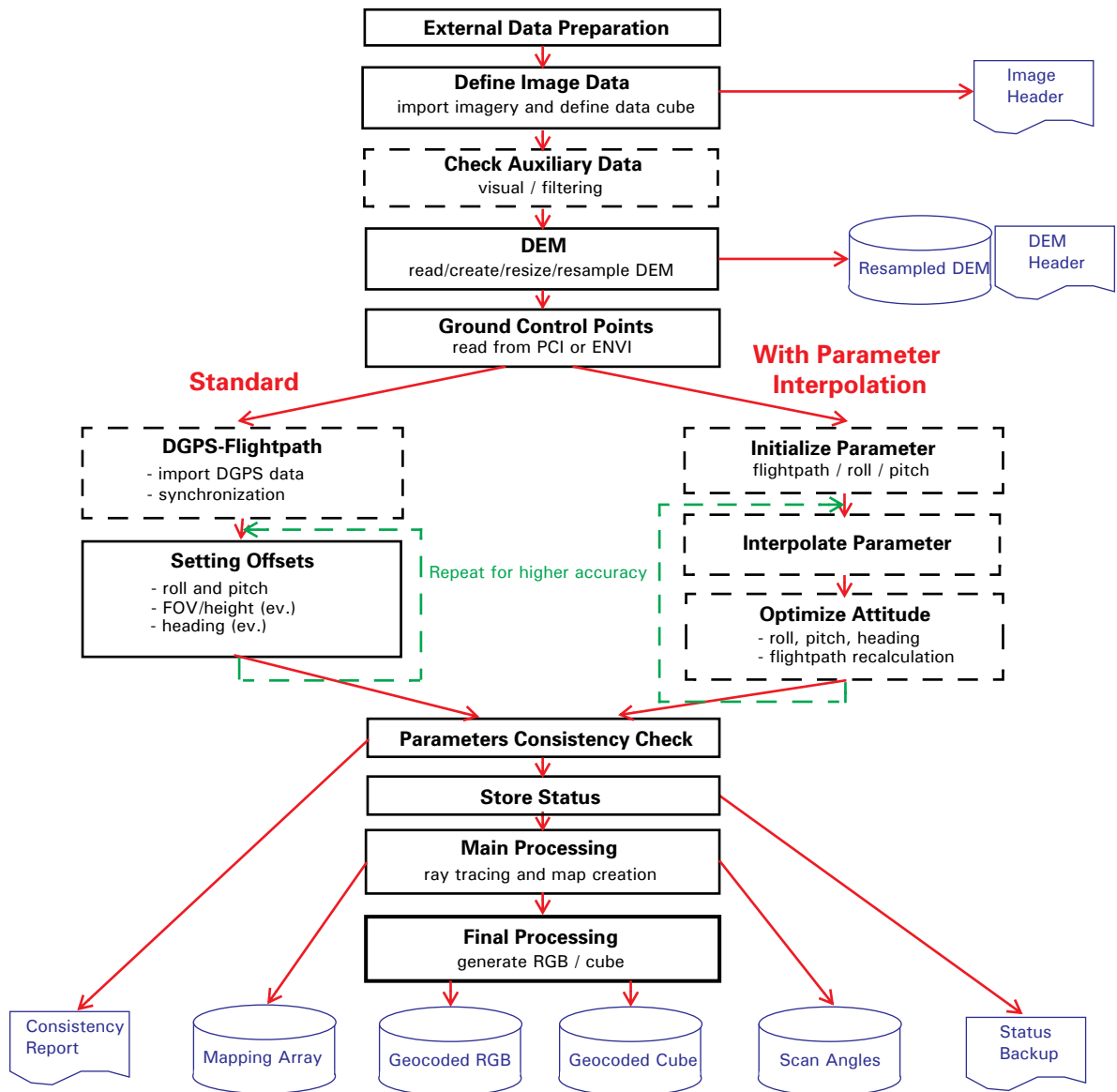


Figure 4: Process data flow of the parametric geocoding as implemented in the PARGE application, from the raw data to the main output files of the process.

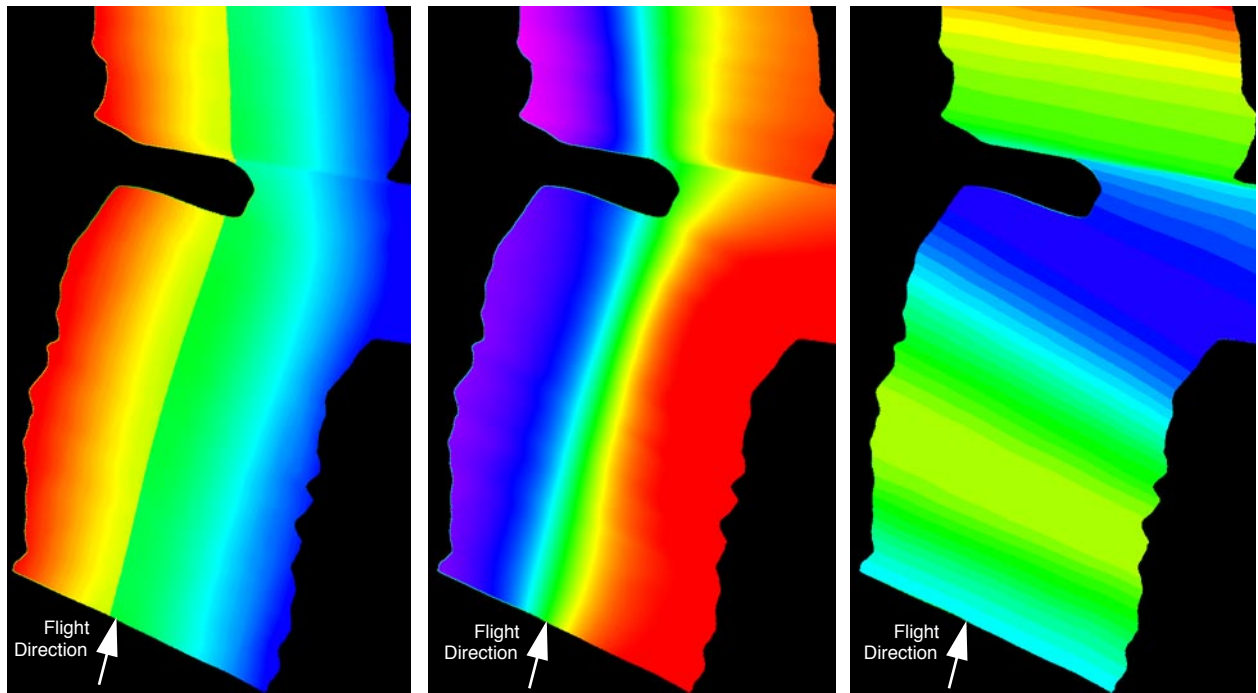


Figure 5: Example of the linking layers for radiometric processing of airborne scanner data: scan zenith (left), azimuth (middle), and aircraft altitude (right). The nadir line appears prominently in the scan zenith due to the negative coding of flight-right hand side pixels. The color coding used is blue for small values, green for intermediate values, and red for large values.

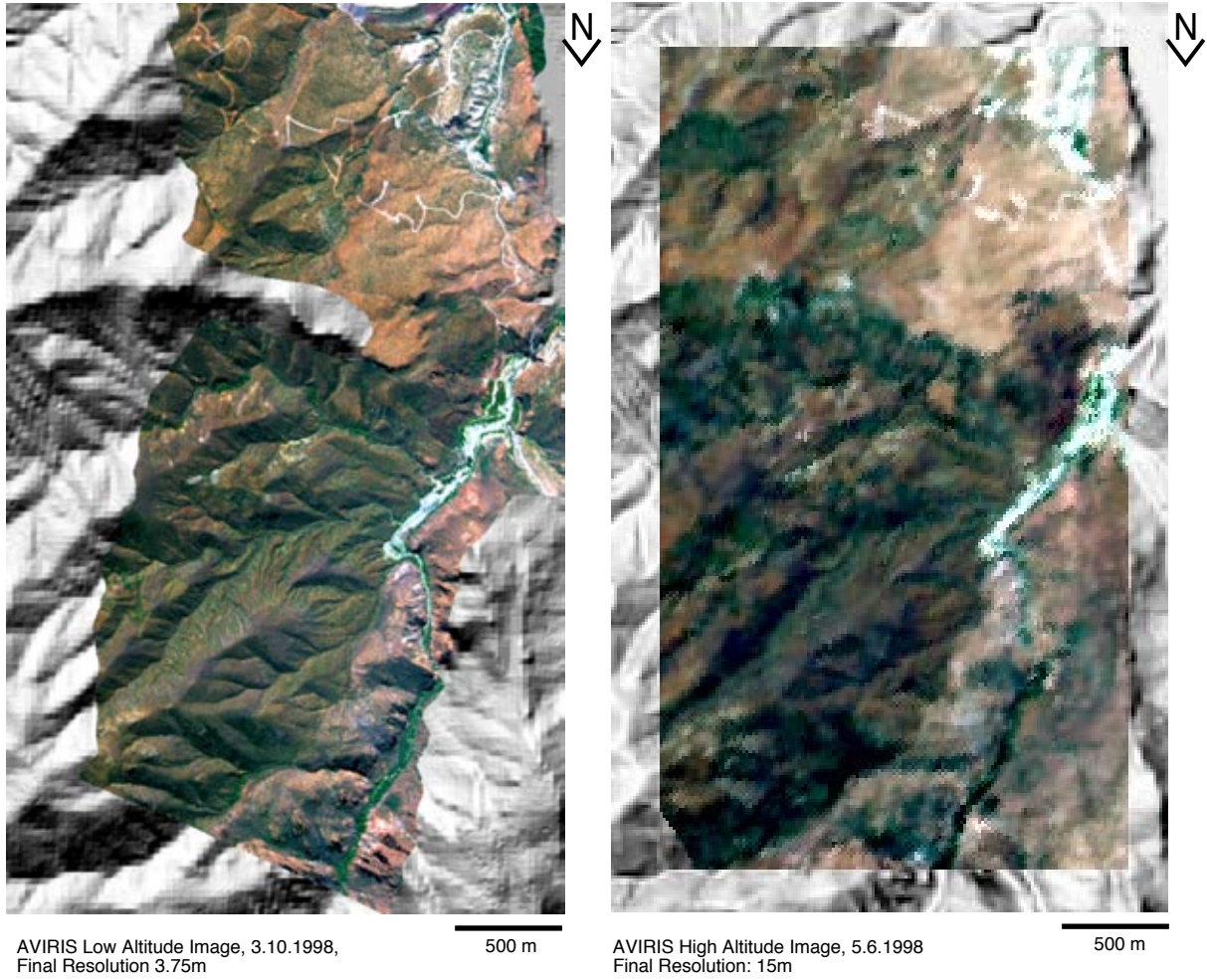


Figure 6: Co-registration data analysis of AVIRIS high altitude and low altitude data in Ray Mine Arizona in relation to the illumination shaded DEM. Overlay of the orthorectified AVIRIS imagery on the ATCOR derived solar illumination map (based on 7.5' USGS DEM). Left: Low altitude data (3.75m resolution); right: High altitude data (15m resolution).

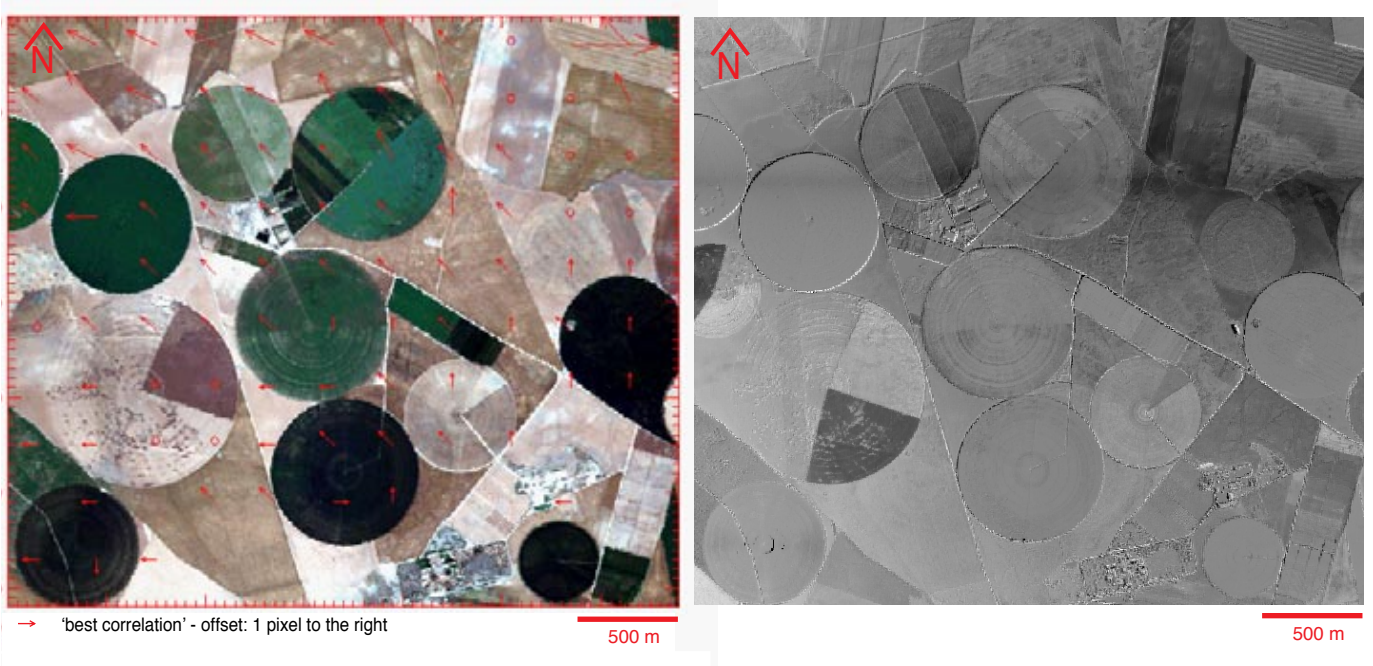


Figure 7: Barrax co-registered HyMap data. Left: Raw data true color image with overlaying offset-arrows. Right: Difference image between north-south and east-west flight including BRDF effects (Hot Spot) and border effects due to the co-registration errors of 1-2 pixels (3.52 x 3.10 km).

LIST OF FIGURES

Figure 1: Rotated sensor coordinate system (x',y',z') in space and the orientation of the attitude angles (ω, φ, κ). The scan vector \vec{L}_i is derived by transformation of the coordinate system.

Figure 2: Intersection procedure of the real scan vector with the DEM.

Figure 3: Error within the PARGE approach with respect to misalignment between sensor model and the attitude measurement unit. The angular difference between the exact solution (offsets directly in the sensor model) and the approximative solution with offset in the roll/pitch angles is depicted.

Figure 4: Process data flow of the parametric geocoding as implemented in the PARGE application, from the raw data to the main output files of the process.

Figure 5: Example of the linking layers for radiometric processing of airborne scanner data: scan zenith (left), azimuth (middle), and aircraft altitude (right). The nadir line appears prominently in the scan zenith due to the negative coding of flight-right hand side pixels. The color coding used is blue for small values, green for intermediate values, and red for large values.

Figure 6: Co-registration data analysis of AVIRIS high altitude and low altitude data in Ray Mine Arizona in relation to the illumination shaded DEM. Overlay of the orthorectified AVIRIS imagery on the ATCOR derived solar illumination map (based on 7.5' USGS DEM). Left: Low altitude data (3.75m resolution); right: High altitude data (15m resolution).

Figure 7: Barrax co-registered HyMap data. Left: Raw data true color image with overlaying offset-arrows. Right: Difference image between north-south and east-west flight including BRDF effects (Hot Spot) and border effects due to the co-registration errors of 1-2 pixels (3.52 x 3.10 km).